Bendola Publishing
Journal of Transition Metal Complexes
Vol. 4 (2021), Article ID 246127, 9 pages
doi:10.32371/jtmc/246127

Research Article

Formulation, Molecular Charge Topography, and Nosocomial Anti-Infectious Potential of Ruthenium Carbonyl Complex of N-*o*-Hydroxyacetophenone-Ethylenediamine-N′-*o*-Vanillin

Jan Mohammad Mir, Neeta Jain, and Ram Charitra Maurya

Coordination, Metallopharmaceutical and Computational Chemistry Laboratory, Department of P. G. Studies and Research in Chemistry and Pharmacy, R. D. University, Jabalpur, M. P., India
Address correspondence to Jan Mohammad Mir, mirjanmohammad@gmail.com

Received 20 May 2021; Revised 4 July 2021; Accepted 9 July 2021

Abstract Nosocomial infections are ranked as the second-largest infections. *E. coli* is the primary causative agent of this dreadful infection. To develop effective antibiotic substances against hospital-acquired infections, herein a novel carbon monoxide tagged Ru(II) complex of N-*o*-hydroxyacetophenone-ethylenediamine-N′-*o*-vanillin is reported as an effective antimicrobial agent of its form. In addition to molecular structure elucidation, an explanation has been made about the related charge topography concerning the biological effect. The formulation of the complex based on hyphenated experimental-theoretical evaluation suggests an octahedral structure. Density functional study was carried out confined to the formalism as B3LYP functional/LanL2DZ basis set for Ru atom and 6–31 g(d,p) for the rest of the atoms. The stable form of geometry and other electron density plots are the prominent inclusions discussed in this work. The primary characterization techniques that have been used for the formulation include elemental analysis, mass spectrometry, nuclear magnetic resonance (C and H), UV-Vis, and FT-IR. The experimentally observed data was validated with theoretical/computational outputs. Both the experimental and theoretical results sound in excellent agreement when compared at each step of the characterization. A suitable trans-octahedral geometry has been suggested for the complex. From the antimicrobial actions against nosocomial *E. coli*, an MIC value of 30 μM was obtained for the selected compound and hence can be assumed as a standard novel antibiotic substance against nosocomial infections. The respective microbial study has been discussed, keeping in view the microbial growth study, the qualitative and quantitative analysis to add fascination to the work being reported.

Keywords RuCO; nosocomial; DFT; spectroscopy

1. Introduction

Ruthenium complexes possess significant properties of medicinal and industrial interest. The effective coordinating behavior with nucleic acids and proteins indicates the bio-conjugation potential of this metal [1]. Ruthenium carbonyl complexes are organometallic compounds possessing well pronounced DNA interacting properties and have flexible redox properties [2]. These compounds serve as critical materials for the synthesis of diversified complexes [3]. The applications towards olefin metathesis and many other catalytic aspects show the industrial importance of such chemicals [4]. The photodynamic role and antimicrobial potential of Ru-compounds are indications of biomedicinal significance [5,6]. The selection of other co-ligands other than CO for metal complexation is always made based on the relevance with applied interest. Bisazomethines represent a highly fascinating class of ligands for displaying excellent metal chelating properties [7,8]. Di-imine-based metal complexes have been reported to show remarkable DNA binding ability [9]. Fluorescent switching properties and ring-opening polymerization (ROP) of lactide have also been reported for similar types of compounds [10,11].

Both *o*-vanillin and *o*-hydroxyacetophenone compounds possess medicinal and industrial significance. *o*-Vanillin shows effective therapeutic relevance [12,13]. The hydroxyl composition in this type of ligand favors efficient insecticidal behavior that has been evaluated at both the experimental and theoretical levels [14]. The effective way shows that amyloid-binding is fascinating in relevance with the study of Alzheimer's disease (AD) treatment [15]. Also, the biological efficacy of this compound is evident from several other bioassays reported recently [16,17]. Another co-ligand, *o*-hydroxyacetophenone, is a noteworthy molecule that exhibits significant material properties [18]. The use of this compound has been found in synthesizing pyrazole derivatives [19]. In association with other ligands, 2-hydroxyacetophenone enhances the luminescence effect and other light-driven interesting properties [20]. The scientific temper regarding the mutational impact and cardiovascular implications determined for these compounds is highly remarkable [21,22]. Such type of Schiff base complexes has been shown to possess well pronounced biological properties [23,24].

Because of the multifold importance of such complexes, this work mainly focuses on the synthesis and combined theoretical-experimental exploration of a ruthenium hydride

carbonyl complex of bisazomethine ligand (ethylenediamine, *o*-vanillin, and *o*-hydroxyacetophenone). Antimicrobial activity of the target compound against hospital-acquired infecting (HAI) microbes is the main applied aspect of this work. Microbial isolation and identification have also been performed, and *E. coli*, the primary causative agent of the said infection, has been targeted.

2. Experimental

2.1. Materials

All the chemicals used for the synthesis of the complex were products of Sigma Aldrich Chemical Co., USA, except Triphenylphosphine that was supplied by Alfa Aesar, UK, and were of analytical reagent grade.

2.2. Physicochemical methods

Infrared spectra were recorded on Bruker FT-IR spectrophotometer using potassium bromide pellets of all the compounds. Electronic spectral analysis was conducted using UV-visible spectrometer (Cary 5000, US). The decomposition temperature was recorded using an electrically operational melting point apparatus (Kumar Industries, Mumbai, India) bearing heating capacity up to 360 °C. NMR, mass spectrometry, and elemental analysis were made available by SAIF-CDRI, Lucknow, India. All solutions were purged with N_2 for half an hour before each experiment.

2.3. Computational methods

The theoretical calculations were run using a licensed Gaussian 09 software package. The complex structure was optimized using LanL2DZ for Ru and 631 g(d,p) for all other atoms invoking B3LYP as functional. The *cis*-CO−PPh_3 and *trans*-CO−PPh_3 forms of the complex were evaluated computationally under DFT investigation using the same formalism. After confirming the absence of imaginary frequency in the generated structures, the resultant optimal conformations were made as input files for the further spectroscopic or other electron density computations following the same calculation scheme as described in the optimization [25,26,27].

2.4. Synthesis

2.4.1. Synthesis of [RuHCl(CO)(PPh$_3$)$_3$]

To a vigorously well stirred 60 mL 2-methoxyethanol hot solution of triphenylphosphine (6.0 mmol), 1 mM ruthenium trichloride dissolved in 2-methoxyethanol (20 mL) was added followed by rapid addition of 20 mL aqueous formaldehyde (40% w/v). The resulting mixture was further heated for 10 m under reflux and was then allowed to cool. A creamy-white precipitate was finally obtained that was washed using water-ethanol, ethanol, and n-hexane as washing agents and dried in vacuum.

Analytical data—Chemical Formula: $C_{55}H_{46}ClOP_3Ru$; Molecular Weight: 952; m/z: 952, 953; Decomposition Temperature: 140 °C; Elemental Analysis Calc./Found (%)—C: 69.36/69.31, H: 4.87/4.89, and O: 1.68/1.63; IR data (cm^{-1})—ν_{CO}: 1,924, ν_{Ru-H}: 2,013, and $\nu_{Ph(P-Ph)}$: 1,432, 1,437. The FT-IR spectrum of the *[RuHCl(CO)(PPh$_3$)$_3$]* is given in Figure S1.

2.4.2. Synthesis of the Schiff base

To a 20 mL ethanolic solution of ethylenediamine (10 mmol, 0.667 mL) 1.2 mL of *o*-hydroxyacetophenone (10 mmol) and 1.52 g of *o*-vanillin (10 mmol) were simultaneously added. The ternary mixture was allowed to reflux for 6 h (constant stirring) to form a yellow solid precipitate. By allowing the reaction vessel to cool and let the solvent get reduced slowly through evaporation at room temperature, finally the compound was washed using ethanol and water as washing agents. The product was dried in vacuum supported by anhydrous calcium dichloride and was recrystallized from ethanol.

Analytical data—Chemical Formula: $C_{18}H_{20}N_2O_3$; Molecular Weight: 312; m/z: 312; Decomposition Temperature: 109 °C; Elemental Analysis Calc./Found (%)—C: 69.21/69.21, H: 6.45/6.43, N: 8.97/8.95, and O: 15.37/15.35, IR data (cm^{-1})—$\nu_{CH=N}$: 1,610, $\nu_{C=N}$: 1,575, $\nu_{(OH)}$: 3,429, 1,444, ν_{C-O}: 1,368, and $\nu_{C=C}$: 1,506.

2.4.3. Synthesis of Ru(II) carbonyl complex of the Schiff base ligand

An amount of 0.994 g (1 mM) of [RuHCl(CO)(PPh_3)$_3$] was dissolved in 20 mL of dichloromethane (DCM) and was purged with nitrogen for 15 m. This was followed by adding 0.312 g of the Schiff base (1 mM). The reaction vessel containing the mixture was put on a magnetic stirrer fitted with heating mantle to reflux under constant stirring for 10 h at 40 °C. This resulted in the formation of bottle green solid precipitate. The solvent was allowed to vaporize to reduce it to a small volume (≈ 3 mL) and the desired product started separating out when a small amount of pet-ether (60–80 °C) was added. The product was filtered, washed (using DCM followed by ether) and was left to dry in anhydrous $CaCl_2$ supported *vacuum*. Recrystallized was done from 1:2 (v:v) chloroform-pet ether (60–80 °C) mixture.

Analytical data—Chemical Formula: $C_{37}H_{33}N_2O_4PRu$; Molecular Weight: 702; m/z: 702, 701, 704, and 700; Decomposition Temperature: 160 °C, Elemental Analysis Calc./Found (%)—C: 63.33/63.30, H: 4.74/4.75, N: 3.99/3.95, and O: 9.12/9.10; IR data (cm^{-1})—ν_{CO}: 1,961, $\nu_{Ph(P-Ph)}$: 1,437, $\nu_{CH=N}$: 1,609, $\nu_{C=N}$: 1,574, ν_{C-O}: 1,381, and $\nu_{C=C}$: 1,513.

The complex was found soluble in acetonitrile, DCM, and dimethyl sulfoxide.

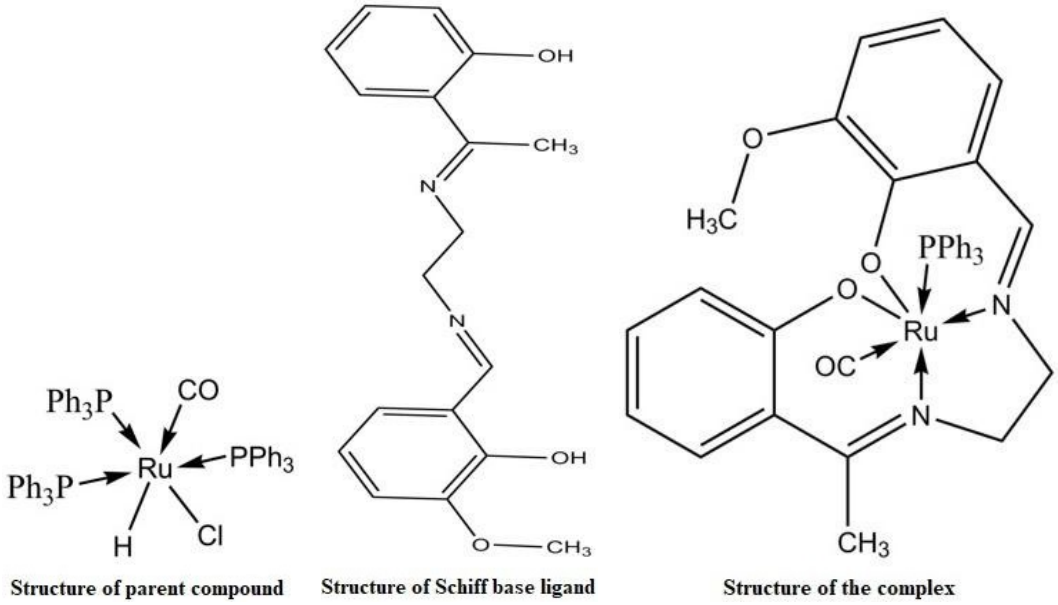

Figure 1: Proposed structure of compounds involved in the study.

3. Results and discussion

3.1. Structural evaluation of the Schiff base

The formation of the Schiff base ligand has been discussed in light of various physicochemical means. From the data formulation of the ligand is in full agreement with the proposed structure. The formula mass is comparable with the results obtained from the respective elemental analysis and mass spectrometry. FT-IR spectral results indicate two significant vibrational modes at 1,610 cm^{-1} and 1,575 cm^{-1}, for $\nu_{CH=N}$ and $\nu_{C=N}$, respectively [19,20, 27]. Other vibrational signatures important in identifying $\nu_{(OH)}$ at 3,429 cm^{-1} and ν_{C-O} at 1,368 cm^{-1} are also clear. ^{1}HNMR spectral analysis shows distinctive resonating signals for enolic protons at 16 ppm. Aromatic protons are well distinguishable at 6.4–7.6 ppm. A feeble 8.2 ppm signal may be assigned for $>$ CH=N$-$ proton, 3.8 ppm for $-OCH_3$ and remaining methyl groups around 2.5 ppm. Similarly, ^{13}CNMR shows $>$ C=N and $-$CH=N$-$ resonating frequency at 163. The existence of C$-$O enolic is confirmed from the appearance of chemical shift of 172 ppm different from $>$ C=O that appears usually at 180 ppm. δ values of the range of 117–132 show aromatic carbons of varied substitution. A 50 ppm signifies the methyl groups of OCH_3 portion of *o*-vanillin moiety, while 14.7–14.8 ppm is meant for ethylene diamine methyl groups. The pentet signal of 2.5 ppm in ^{1}HNMR and a septet signal near 78 ppm denote solvent signals of DMSO-d_6 used in the experiment. The Schiff base related FT-IR, ESI-mass and NMR spectra are shown in Figures S2–S4. Figure 1 shows the proposed 2D structure of the compounds in the present investigation along with the structure of the ligand [19,20,27].

3.2. DFT-based justification of cis versus trans forms of the complex

In order to remain confined to a single isomeric form of the complex, DFT-based evaluation of both the *cis*- and *trans*-forms of the complex with respect to (CO)(PPH_3) was first of all determined. The respective optimized structures have been given in Figure 2. The total energy continum (E_{total}), zero point energies (ZPE) and frontier orbital energies (FOE) show that trans-isoform is thermodynamically more stable as compared to the *cis*-form. E_{total}, ZPE, and FOE for *cis*-complex come out to be $-2,275.57$ au, 387.09 Kcal/mole, and 3.65 eV (HOMO-LUMO gap), respectively, whereas the calculation for the same descriptors of the *trans*-isomer shows E_{total}, ZPE, and FOE to be $-2,275.55$ au, 386.67 Kcal/mole, and 3.69 eV. Therefore, it is logical to state here that the DFT structural investigation shall involve mainly the data obtained for the trans-isoform of the complex.

3.3. Structural verification of the complex

The consistency of analytical data with the proposed structure (Figure 1) of the complex is clearly showing an excellent agreement with the theoretical outcomes. In the FT-IR spectrum (Figure S5) of respective complex, ν_{CO}: 1,961 cm^{-1}, $\nu_{Ph(P-Ph)}$: 1,437 cm^{-1}, $\nu_{CH=N}$: 1,609 cm^{-1}, $\nu_{C=N}$: 1,574 cm^{-1}, ν_{C-O}: 1,381 cm^{-1}, and $\nu_{C=C}$: 1,513 cm^{-1} shows the excellent binding ability of Schiff base ligand under discussion and the presence of PPh_3 and CO as co-ligands. The resemblance between the experimental and computed IR data may be also seen as shown in Figure S5.

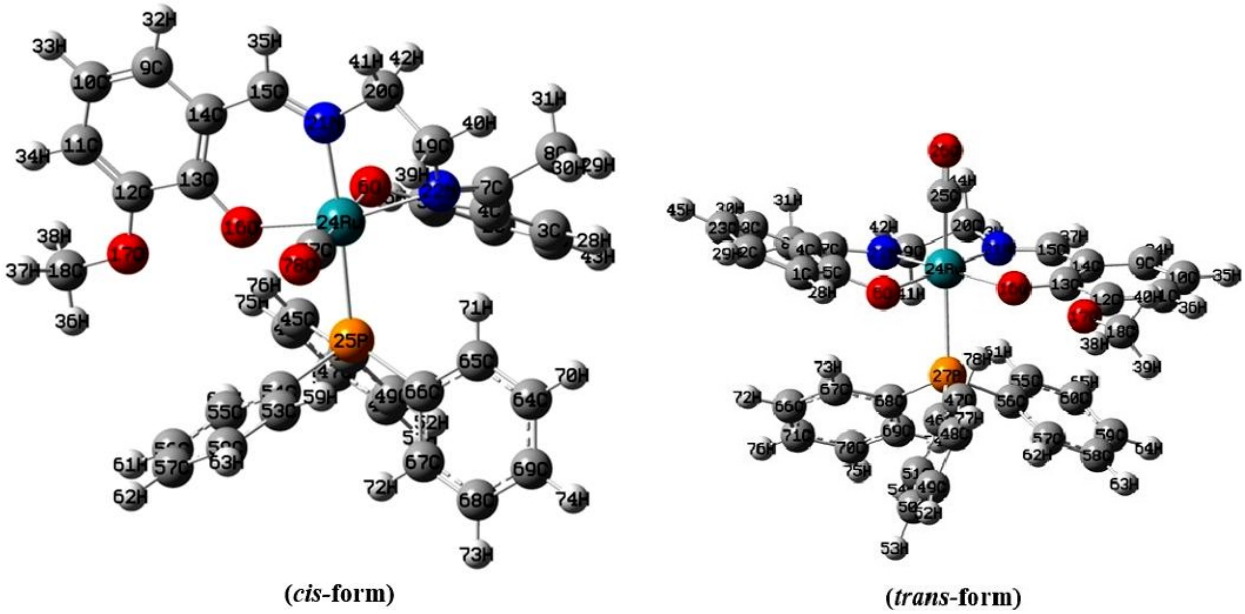

Figure 2: Optimized structural isoforms of the complex.

UV-Vis spectroscopic details of the ruthenium(II) complex clearly indicate the excellent mode of binding between target ligand and the metallic core. The central metal has been found to be diamagnetic indicating the presence of ruthenium in II oxidation state. The ground state of ruthenium(II) ($t^6{}_{2g}$ configuration) is $^1A_{1g}$. The excited states corresponding to $t^5{}_{2g}\ e^1{}_g$ configuration are $^3T_{1g}$, $^3T_{2g}$, $^1T_{1g}$, and $^1T_{2g}$ in the order of increasing energy. This speculates the existence of four bands corresponding to the transitions from $^1A_{1g}\rightarrow{}^3T_{1g}$, $^3T_{2g}$, $^1T_{1g}$ or $^1T_{2g}$ (in the order of increasing energy). The electronic spectrum of the complex was recorded in DMSO using 1 mM solution. The respective electronic spectrum of the complex shows four to five bands in the region 210–550 nm. The bands appearing at 210 nm and 317 nm may be assigned due to $\pi \rightarrow \pi^*$ and $n \rightarrow \pi^*$ transitions, respectively. The solvent shows a slight effect on the band positions exhibiting bands around 430–550 nm, which could be assigned to charge transfer transition of an electron from the metal t_{2g} level to an unfilled molecular orbital derived from the π^* level of the CO [28]. This assignment is similar to assignments made for similar other ruthenium(II) octahedral complexes [29]. The observed multiple absorptions prove the presence of different acceptor levels in the complex.

TD-DFT electronic spectral speculation displaying nonzero oscillatory strengths (f) show that the results are acceptable and possess considerable absorption peaks. From f values 0.001 to 0.0481 it is clear that the involved transitions are spin allowed transitions and are d-p mixing and charge-transfer type [30]. Theoretical spectrum may be used to validate the experimental observation. It is clear from Figure S6 that the applied theory in evaluating TD-DFT electronic excitation parameters are in good agreement with what was observed experimentally. The calculation involves three levels of excitation involving the respective wavelength, the energy of excitation, and the probability of excitation to occur among all the given possible transitions. It may be mentioned here that total energy, E(TD-HF/TD-KS) $= -2275.40$ a.u., meant for the state of optimization and/or second-order correction was the over-all result for the single point energy calculation. The theoretical UV-Vis data involving the energies of excitation and the excitation coefficients are given in Table 1. The excitation coefficient serves as a speculative tool to find the most probable transitions possible in the complex. The square of the coefficient multiplied by a factor of 200 gives the percentage contribution of an electronic transition. It is HOMO-LUMO transition that has been computed to be most probable. Other transitions also tend towards visible region. From the frontier orbital analysis (*Vide infra*) the HOMO-LUMO gap is quite low as compared to the coordinated ligands. Moreover, from the theoretical infrared spectral insight (*vide supra*) it is Ru−CO bond that needs around 6 KJ/mol only for its bond with metal to vibrate. Hence, one may speculate it here that all the spectral data present a predictive vision that the CO ligand will be experienced as fast and foremost releasing group and that too at the expenses of visible form of energy [31, 32, 33].

Mass spectrum of the complex is shown in Figure S7. The expected formula mass of the compound is directly fetchable from the spectrum. Almost the molecular weight

Table 1: Theoretical UV-Vis data of the complex.

Assignment of excited state (ES)	Energy of excitation, λ_{max} and oscillator strength	Orbital assignment	Excitation coefficient
ES1	2.85 eV, 434.25 nm ($f = 0.0322$)	HOMO-2 → LUMO	−0.10
		HOMO-1 → LUMO	−0.20
		HOMO → LUMO	0.65
ES2	2.96 eV, 419.40 nm ($f = 0.0262$)	HOMO-2 → LUMO+1	−0.13
		HOMO-1 → LUMO+1	−0.23
		HOMO → LUMO+1	0.63
ES3	3.10 eV, 399.82 nm ($f = 0.0110$)	HOMO-2 → LUMO	0.32
		HOMO-1 → LUMO	0.53
		HOMO → LUMO	0.21
ES4	3.13 eV, 395.46 nm ($f = 0.0075$)	HOMO → LUMO+2	0.50
		HOMO → LUMO+4	0.26
		HOMO → LUMO+6	0.12
ES5	3.20 eV, 387.27 nm ($f = 0.0091$)	HOMO-1 → LUMO+1	0.49
		HOMO-2 → LUMO+1	0.34
		HOMO → LUMO+1	0.25
ES6	3.39 eV, 365.69 nm ($f = 0.0043$)	HOMO-2 → LUMO+2	0.29
		HOMO-2 → LUMO+4	0.17
		HOMO-1 → LUMO+2	0.37
ES7	3.43 eV, 361.07 nm ($f = 0.0235$)	HOMO-2 → LUMO	0.56
		HOMO-1 → LUMO	−0.35
ES8	3.49 eV, 354.76 nm ($f = 0.0041$)	HOMO → LUMO+2	−0.34
		HOMO → LUMO+4	0.40
ES9	3.55 eV, 349.32 nm ($f = 0.0481$)	HOMO-2 → LUMO+1	0.54
		HOMO-1 → LUMO+1	−0.38
ES10	3.57 eV, 347.50 nm ($f = 0.0014$)	HOMO → LUMO+2	0.18
		HOMO → LUMO+3	0.47

of 702 with a distinctive stretch of certain units certifies the isotopic forms of the complex in respect to Ru element. The m/z value of 312 and 313 may be assigned for the presence of Schiff base ligand. All other fragments having existence below 5% were ignored.

From the NMR analysis (Figure S8) of the complex again the certainty of proposed formula of the complex is established. The absence of enolic signals in the respective ^{1}HNMR spectrum of complex clarifies the coordination of respective Schiff base. Moreover, the recurrence of important resonating frequencies when compared with the respective Schiff base again stems the successful binding. Similarly, in case of ^{13}CNMR spectrum, it details the presence of coordinated carbonyl group and also shows the presence of other carbon atoms. For example, 170 ppm is meant for coordinated CO, 161 denotes the resonance of enolic carbon, and the signals at 12 and 48 show the presence of methyl groups [34].

3.4. DFT-based theoretical studies

The various bond lengths, bond angles, and dihedral angles generated from the equilibrium structure of the *trans*-form of the complex are given in Table 2. The results obtained for the geometry of the complex are in good agreement with the similar type of metallic systems reported elsewhere [35].

Table 2: Selected geometrical optimization parameters of the complex.

Atom connectivity	Bond length (Å)	Atom connectivity	Bond angle (°)
O(16)—Ru(24)	2.12	N(22)—Ru(24)—C(25)	167.04
P(27)—Ru(24)	2.40	N(21)—Ru(24)—P(27)	165.68
O(6)—Ru(24)	2.14	O(16)—Ru(24)—O(6)	177.44
C(25)—Ru(24)	1.87	O(16)—Ru(24)—C(25)	91.50
N(21)—Ru(24)	2.14	P(27)—Ru(24)—C(25)	90.75
N(22)—Ru(24)	2.20	O(6)—Ru(24)—P(27)	93.58
		N(22)—Ru(24)—O(6)	77.86
		N(21)—Ru(24)—N(22)	77.36
		N(21)—Ru(24)—O(16)	81.88

Atom connectivity	Dihedral angle (°)
N(22)—Ru(24)—C(25)—O(26)	23.57
N(22)—Ru(24)—P(27)—H(46)	−100.55
N(22)—Ru(24)—O(6)—C(5)	135.31
N(21)—Ru(24)—N(22)—C(7)	−142.47
N(21)—Ru(24)—O(16)—C(13)	51.91
C(13)—O(16)—Ru(24)—C(25)	−45.74
O(26)—C(25)—Ru(24)—O(16)	172.60
Ru(24)—N(21)—C(20)—C(19)	−47.62

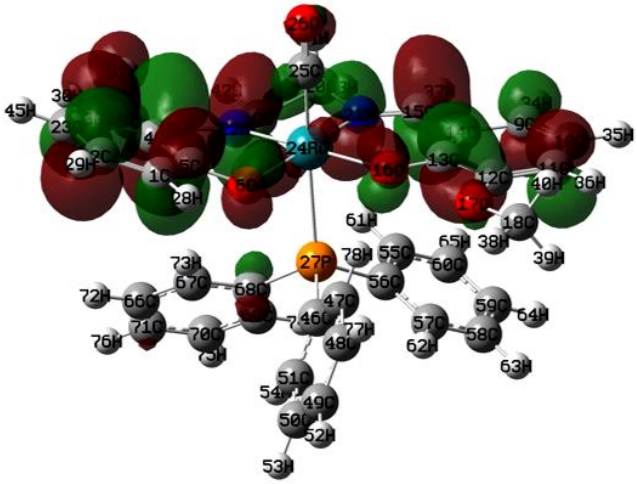

Figure 3: MO (mixed HOMO-LUMO) diagram of the complex.

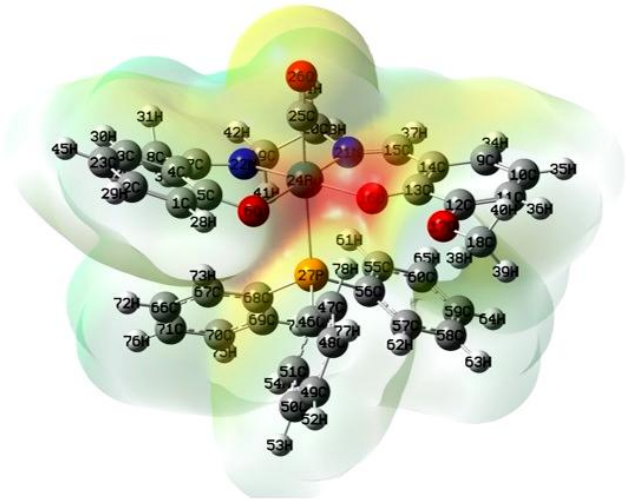

Figure 4: Electrostatic potential surface of the complex.

An octahedral geometry is proposed for the complex and is eminent from the optimized parameters. After serious examination of the metallic coordination zone it may be enunciated that Ru−CO link bears different electronic property as compared to other connectivites under question. It clarifies the assumption of Ru−CO tendency to behave as the foremost locus to any chemical change. Refer to Figure 2 for the numerical assignments made for the *trans*-isomer.

3.5. FMO analysis

Frontier orbitals are very important characterizing tools for chemical reaction [36]. It can help in predicting feasibility of a chemical process. Hence, they are called the Frontier orbitals. The HOMO primarily acts as an electron donor and the LUMO hence the acceptor, and the gap between HOMO and LUMO characterizes the molecular chemical stability [37]. The electronic fillings of MO's in complex verify their diamagnetic behavior. The frontier orbitals that were computed have been shown along with the energy gaps in Figure 3. From the HOMO-LUMO gap of compound, the energy dissipation may be proven helpful in terms of charge delocalization along alternative signal and double bonds. The persistence of LUMO towards CO ligand may be sought in designing the locus to stimulate the compound to release CO.

3.6. MESP and antibacterial activity

Molecular electrostatic potential surface as obtainable from theoretical graphics helps a lot in understanding the potentiality towards biological relevance [38,39,40,41]. The distinctive red, blue, and neural zones as shown in Figure 4 explain the prediction of this property. Keeping in view the appearance of these three spots on the surface diagram, it is easy to establish the cell permeability of the compound. This can be further explained based on electrophilic and nucleophilic zones within the complex. From Mulliken charge analysis O-6, O-16, O-17, O-26, C-8, C-9, C-10, C-11, C-18, C-19, C-20, C-23, N-21, and N-22 represent components of nucleophilic zone, whereas the rest of the atoms constitute the electrophilic region. Such a potential varying justification helps to explain the reactive behavior towards a biological membrane. The emphasis given upon the electrostatic interaction of Ru-core with regard to cellular DNA binding and cell wall traversing phenomenon can thus be inferred computationally.

3.7. Microbial growth, qualitative and quantitative analysis

The hospital origin samples were collected from Bombay Hospital Jabalpur and were cultured and identified in the Microbiology Department of our university. Disposed catheters and urine samples were collected from UTI-infected persons from Mumbai Hospital, Jabalpur, India. The microbial culture, identification, and antibacterial activity were experimented at Biological Science Department, R. D. University, Jabalpur, India. The results in the form of zone inhibition were measured in mm. The microorganisms present in urine samples of CAUTI infected patients were cultured in the nutrient broth and were differentiated using the gram staining procedure into gram positive and gram negative organisms. The organisms were transferred to cystine lactose electrolyte deficient (CLED) agar medium for further differentiation of urinary organisms. Urine samples were shaken well in their containers for even distribution of bacteria. A calibrated wire loop with internal diameter 3.26 mm that hold 0.004 mL of urine was inoculate into the above media. The inoculums were spread with the wire loop on the media plate. Plates were incubated aerobically at 37 °C for 24 h. Pure isolated colonies were Gram differentiated and then biochemically identified. The biochemical

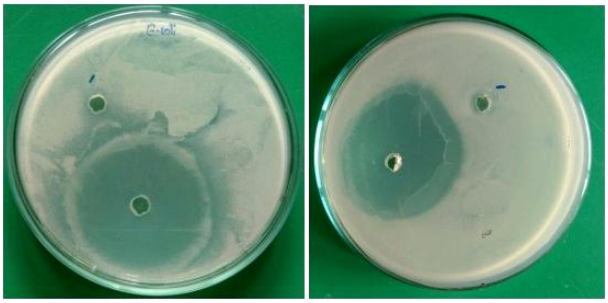

Figure 5: Petri-plates showing inhibition zones against *E. coli*.

tests that were performed for each organism including catalase activity, indole production test, citrate utilization test, and urease test were done for identification. Results from the present study showed that 85% bacterial isolates comprise of 50% nonpathogenic bacteria, 37% pathogenic bacteria, and remaining No Bacteria Growth (NBG). The sampling showed that *S. aureus*, *E. coli*, and *P. aureginosa* were the main pathogenic isolates having existence as 49%, 38%, and 13%, respectively. Urinary samples and catheters almost acted as equal sources of pathogenic bacteria.

3.8. Antibacterial activity

After confirmation of identity of *E. coli* (MTCC 1304), the respective microorganism being the main second causative agent of this infection was selected for the study. The in vitro biological screening effects of the complex at different concentrations by agar well diffusion method were carried out at Bioscience Department, R. D. University, Jabalpur, India. All the experiments were made in triplicates to arrive at the minimum inhibition concentration (MIC) values of the complex [42]. The results in the form of zone inhibition were measured in mm for 20 μM, 40 μM, and 60 μM solutions of the complex, parent compound, Schiff base ligand, and standard drug (tetracycline). In order to obtain MIC value, the control DMSO was separately tested that has shown negligible activity. It was observed that the metal complex shows much more activity in comparison to ligand, standard drug (tetracycline), and the respective parent compound due to the enhanced lipophilicity of the complex (Figure 5). The results have been comparatively presented in Table 3. MIC value shown by the complex is thus 30 μM.

The screening tests have thus shown that metal carbonyl complex possesses the highest activity index as compared to other molecular species under the present investigation. The remarked activity against gram negative species culminates the relevance of polyoxy millieu with the cell wall structure [43,44]. The respective activity index can be calculated by the following relation:

$$\text{Activity index (A.I.)} = \frac{\text{Inhibition zone of sample (mm)}}{\text{Inhibition zone of standard (mm)}}.$$

Table 3: Antibacterial data of the complex and the standard drug (concentration vs. inhibition zones).

Concentration (μM)	Inhibition zone (mm) by standard drug	Inhibition zone (mm) by the complex
20	50	51
40	70	72
60	83	84

From A.I. value of > 1, it can be concluded that the complex is more active as compared to the standard drug employed in the study. Presence of carbon monoxide together with the bioactive components of the complex can be used in immunotherapy. Antibody collection is a laborious task. However, such compounds are engineered to behave as antibiotics of interesting choice. Further stretch in their composition like immunogenic peptides can be brought up by chemical transformation methods. Seeking drugs under this heading may bring forth great approach to treat multidrug resistant microbes causing nosocomial and community acquired infections. The increasing incidence of drug resistant pathogens has developed interest towards compounds that becoming useful therapeutic tools. Briefly, it may be stated that there is a lot yet to be done to explore anti-infectious potential of the metallic complexes in this regard by altering the nature of ligand around the coordination zone. Such results are comparable to the gasotransmitter models reported elsewhere [40,41,45,46,47,48].

4. Conclusions

Quantum chemical calculations are an excellent tool to predict the CO-release of the target complex. The overall characterization techniques have enabled us to declare the complex as bearing an octahedral diamagnetic property having a good level of antibacterial potentiality and CO-releasing ability/lability at a feasible energy range. Theoretical and experimental results have shown excellent agreement with one another. From the antimicrobial action against nosocomial *E. coli*, an MIC value of 30 μM was obtained for the selected compound and hence can be assumed as a standard novel antibiotic substance against nosocomial infections. Other isolated microbes can also be tested similarly. The overall impact of ligands coordinated with metal-carbonyl core can be suggested as a future tool to exaggerate the study of this form. The same complex can also be tested against clinically isolated microbes other than *E. coli* to expand the targeted theme.

Acknowledgments Analytical facilities were provided by the Central Drug Research Institute, Lucknow, India, and the Regional Sophisticated Instrumentation Centre, Indian Institute of Technology, Mumbai, India, are gratefully acknowledged.

For supplemental material refer to Figures S1–S8.

Conflict of interest The authors declare that they have no conflict of interest.

References

[1] M. Flamme, E. Clarke, G. Gasser, and M. Hollenstein, *Applications of ruthenium complexes covalently linked to nucleic acid derivatives*, Molecules, 23 (2018), 1515.

[2] A. Jain, N. T. Garrett, and Z. P. Malone, *Ruthenium-based photoactive metalloantibiotics*, Photochem Photobiol (to appear).

[3] M. Marloye, H. Inam, C. J. Moore, V. Debaille, J. R. Pritchard, M. Gelbcke, et al., *Synthesis, structure and anticancer properties of new biotin- and morpholine-functionalized ruthenium and osmium half-sandwich complexes*, J Biol Inorg Chem (to appear).

[4] E. Păunescu, G. Boubaker, O. Desiatkina, N. Anghel, Y. Amdouni, A. Hemphill, et al., *The quest of the best—A SAR study of trithiolato-bridged dinuclear Ruthenium(II)-Arene compounds presenting antiparasitic properties*, Eur J Med Chem, 222 (2021), 113610.

[5] J. M. Mir, N. Jain, P. S. Jaget, and R. C. Maurya, *Density functionalized [Ru^{II}(NO)(Salen)(Cl)] complex: Computational photodynamics and in vitro anticancer facets*, Photodiagnosis Photodyn Ther, 19 (2017), 363–374.

[6] K. Murugan, S. Vijayapritha, V. Kavitha, and P. Viswanathamurthi, *Versatile formation of Ru(II) hydrazone complexes: Structure, theoretical studies and catalytic activity in α-alkylation*, Polyhedron, 190 (2020), 114737.

[7] S. A. Majid, J. M. Mir, S. Paul, M. Akhter, H. Parray, R. Ayoub, et al., *Experimental and molecular topology-based biological implications of Schiff base complexes: a concise review*, Rev Inorg Chem, 39 (2019), 113–128.

[8] S. Hopff, L. A. Onambele, M. Brandenburg, A. Berkessel, and A. Prokop, *Discovery of a cobalt (III) salen complex that induces apoptosis in Burkitt like lymphoma and leukemia cells, overcoming multidrug resistance in vitro*, Bioorg Chem, 104 (2020), 104193.

[9] S. Hopff, Q. Wang, C. Frias, M. Ahrweiler, N. Wilke, N. Wilke, et al., *A metal-free salalen ligand with anti-tumor and synergistic activity in resistant leukemia and solid tumor cells via mitochondrial pathway*, J Cancer Res Clin Oncol, 147 (2021), 2591–2607.

[10] S. Di Bella, *Lewis acidic zinc(II) salen-type Schiff-base complexes: sensing properties and responsive nanostructures*, Dalton Trans, 50 (2021), 6050–6063.

[11] M. Strianese, D. Pappalardo, M. Mazzeo, M. Lamberti, and C. Pellecchia, *Salen-type aluminum and zinc complexes as two-faced janus compounds: contribution to molecular sensing and polymerization catalysis*, Dalton Trans, 49 (2020), 16533–16550.

[12] V. F. Salau, O. L. Erukainure, K. A. Olofinsan, and M. S. Islam, *Vanillin exerts therapeutic effects against hyperglycemia-altered glucose metabolism and purinergic activities in testicular tissues of diabetic rats*, Reprod Toxicol, 102 (2021), 24–34.

[13] R. Tiwari, A. Chourasia, A. Chaturvedi, A. Ganeshpurkar, and N. Dubey, *Evaluation of hepatoprotective effect of vanillin in isoniazid-rifampicin induced hepatocellular damage*, Free Radic Antioxid, 10 (2020), 42–46.

[14] C. B. Xue, L. Zhang, W. C. Luo, X. Y. Xie, L. Jiang, and T. Xiao, *3D-QSAR and molecular docking studies of benzaldehyde thiosemicarbazone, benzaldehyde, benzoic acid, and their derivatives as phenoloxidase inhibitors*, Bioorg Med Chem, 15 (2007), 2006–2015.

[15] M. Necula, R. Kayed, S. Milton, and C. G. Glabe, *Small molecule inhibitors of aggregation indicate that amyloid β oligomerization and fibrillization pathways are independent and distinct*, J Biol Chem, 282 (2007), 10311–10324.

[16] V. M. Nurchi, J. I. Lachowicz, G. Crisponi, S. Murgia, M. Arca, A. Pintus, et al., *Kojic acid derivatives as powerful chelators for iron(III) and aluminium(III)*, Dalton Trans, 40 (2011), 5984–5998.

[17] P. Lavaee, H. Eshtiagh-Hosseini, M. Housaindokht, J. Mague, A. Esmaeili, and K. Abnous, *Synthesis, characterization and fluorescence properties of Zn(II) and Cu(II) complexes: DNA binding study of Zn(II) complex*, J Fluoresc, 26 (2016), 333–344.

[18] M. Y. Merza and M. F. El-Bermani, *Estimations of excited state dipole moments of conformers in some o-substituted acetophenones by solvato-chromic shifts*, Spectrochim Acta A Mol Biomol Spectrosc, 60 (2004), 1677–1683.

[19] J. M. Mir, S. Roy, P. K. Vishwakarma, and R. C. Maurya, *cis-Dioxomolybdenum(VI) complex of N-o-hydroxyacetophenoneneisonicotinic acid hydrazide as nosocomial anti-infectious agent: experimental and theoretical study*, J Chin Adv Mater Soc, 6 (2018), 282–300.

[20] J. M. Mir, N. Jain, B. A. Malik, R. Chourasia, P. K. Vishwakarma, D. K. Rajak, et al., *Urinary tract infection fighting potential of newly synthesized ruthenium carbonyl complex of N-dehydroacetic acid-N′-o-vanillin-ethylenediamine*, Inorganica Chim Acta, 467 (2017), 80–92.

[21] R. Zhang, Y. Geng, Y. Xu, W. Zhang, S. Wang, and R. Xiao, *Carbonyl reductase SCRII from Candida parapsilosis catalyzes anti-Prelog reaction to (S)-1-phenyl-1,2-ethanediol with absolute stereochemical selectivity*, Bioresour Technol, 102 (2011), 483–489.

[22] D. Gabriel, L. Pontes, J. da Silva, R. Sudo, M. Corrêa, A. Pinto, et al., *Pharmacological activity of novel 2-hydroxyacetophenone isatin derivatives on cardiac and vascular smooth muscles in rats*, J Cardiovasc Pharmacol, 57 (2011), 20–27.

[23] R. R. Zaky, K. M. Ibrahim, and I. M. Gabr, *Bivalent transition metal complexes of o-hydroxyacetophenone [N-(3-hydroxy-2-naphthoyl)] hydrazone: spectroscopic, antibacterial, antifungal activity and thermogravimetric studies*, Spectrochim Acta A Mol Biomol Spectrosc, 81 (2011), 28–34.

[24] N. Al-Shaalan, *Synthesis, characterization and biological activities of Cu(II), Co(II), Mn(II), Fe(II), and UO_2(VI) complexes with a new Schiff base hydrazone: O-hydroxyacetophenone-7-chloro-4-quinoline hydrazone*, Molecules, 16 (2011), 8629–8645.

[25] M. J. Frisch, G. W. Trucks, H. B. Schlegel, G. E. Scuseria, M. A. Robb, J. R. Cheeseman, et al., *Gaussian 09, Revision C.01*, Gaussian, Inc., Wallingford, CT, 2009.

[26] R. D. Dennington, T. A. Keith, and J. M. Millam, *Gaussview 5.0.8*, Gaussian, Inc., Pittsburgh, PA, 2008.

[27] L. R. Holloway, A. J. Clough, J. Y. Li, E. L. Tao, F. M. Tao, and L. Li, *A combined experimental and theoretical study of dinitrosyl iron complexes containing chelating bis(diphenyl)phosphinoX (X = benzene, propane and ethylene): X-ray crystal structures and properties influenced by the presence or absence of π-bonds in chelating ligands*, Polyhedron, 70 (2014), 29–38.

[28] S. Selvamurugan, P. Viswanathamurthi, A. Endo, T. Hashimoto, and K. Natarajan, *Synthesis, spectral characterization, antioxidant, anticancer in vitro, and DNA cleavage studies of a series of ruthenium(II) complexes bearing Schiff base ligands*, J Coord Chem, 66 (2013), 4052–4066.

[29] A. B. P. Lever, *Inorganic Electronic Spectroscopy*, vol. 33 of Studies in Physical and Theoretical Chemistry, Elsevier, Amsterdam, 1984.

[30] M. C. Day and J. Selbin, *Theoretical Inorganic Chemistry*, East-West Press, New Delhi, 2nd ed., 1985.

[31] Y. Hoshino, *Molecular design for long-range electronic communication between metals*, Platin Met Rev, 45 (2001), 2–11.

[32] R. Prabhakaran, S. Anantharaman, M. Thilagavathi, M. V. Kaveri, P. Kalaivani, R. Karvembu, et al., *Preparation, spectroscopy, EXAFS, electrochemistry and pharmacology of new ruthenium(II) carbonyl complexes containing ferrocenylthiosemicarbazone and triphenylphosphine/arsine*, Spectrochim Acta A Mol Biomol Spectrosc, 78 (2011), 844–853.

[33] M. I. F. Barbosa, R. S. Correa, T. M. Bastos, L. V. Pozzi, D. R. M. Moreira, J. Ellena, et al., *Structural isomerism of*

Ru(II)-carbonyl complexes: synthesis, characterization and their antitrypanosomal activities, New J Chem, 41 (2017), 4468–4477.

[34] E. K. Beloglazkina, A. G. Majouga, E. A. Manzheliy, A. A. Moiseeva, Y. V. Lin'kova, and N. V. Zyk, *Mononuclear ruthenium(II) and rhodium(III) complexes with S-[4-(2,2:6′,2″-terpyridin-4′-yl)phenoxy]butyl ethanethioate and 4′-[4-(1,2-dithiolane-3-yl)butylcarboxy)phenyl]-2,2′:6′,2″-terpyridine: Synthesis, electrochemistry, antibacterial activity and catalytical application*, Polyhedron, 85 (2015), 800–808.

[35] J. G. Hernández, C. A. Huerta-Aguilar, P. Thangarasu, and H. Höpfl, *A ruthenium(III) complex derived from N,N′-bis(salicylidene)ethylenediamine as a chemosensor for the selective recognition of acetate and its interaction with cells for bioimaging: experimental and theoretical studies*, New J Chem, 41 (2017), 10815–10827.

[36] P. H. Amith Nayak, H. S. Bhojya Naik, H. B. Teja, B. R. Kirthan, and R. Viswanath, *Synthesis, characterization and luminescent properties of mixed-ligand nickel complexes for opto-electronic application*, J Electron Mater, 50 (2021), 2090–2100.

[37] T. Chaudhary, M. Chaudhary, and B. Joshi, *Topological and reactivity descriptor of carisoprodol from DFT and molecular docking approach*, J Inst Sci Technol, 26 (2021), 74–82.

[38] F. Li, J. G. Collins, and F. R. Keene, *Ruthenium complexes as antimicrobial agents*, Chem Soc Rev, 44 (2015), 2529–2542.

[39] J. M. Mir and F. A. Itoo, *Experimental-DFT interface of hydrogen bonding description of 1:10 methanol-water solution*, J Mol Liq, 247 (2017), 1–5.

[40] J. M. Mir, S. A. Majid, and A. H. Shalla, *Enhancement of Schiff base biological efficacy by metal coordination and introduction of metallic compounds as anticovid candidates: a simple overview*, Reviews in Inorganic Chemistry (to appear).

[41] J. M. Mir and R. C. Maurya, *Physiological and pathophysiological implications of hydrogen sulfide: a persuasion to change the fate of the dangerous molecule*, J Chin Adv Mater Soc, 6 (2018), 434–458.

[42] J. M. Mir, N. Jain, P. S. Jaget, W. Khan, P. K. Vishwakarma, D. K. Rajak, et al., *Urinary tract anti-infectious potential of DFT-experimental composite analyzed ruthenium nitrosyl complex of N-dehydroacetic acid-thiosemicarbazide*, J King Saud Univ Sci, 31 (2019), 89–100.

[43] A. F. Shoair, A. R. El-Shobaky, and H. R. Abo-Yassin, *Synthesis, spectroscopic characterization, catalytic and antibacterial studies of ruthenium(III) Schiff base complexes*, J Mol Liq, 211 (2015), 217–227.

[44] P. Chuklin, V. Chalermpanaphan, T. Nhukeaw, S. Saithong, K. Chainok, S. Phongpaichit, et al., *Synthesis, X-ray structure of organometallic ruthenium (II) p-cymene complexes based on P- and N- donor ligands and their in vitro antibacterial and anticancer studies*, J Organomet Chem, 846 (2017), 242–250.

[45] R. C. Maurya, P. K. Vishwakarma, J. M. Mir, and D. K. Rajak, *Oxidoperoxidomolybdenum(VI) complexes involving 4-formyl-3-methyl-1-phenyl-2-pyrazoline-5-one and some β-diketoenolates*, J Therm Anal Calorim, 124 (2016), 57–70.

[46] J. M. Mir, R. C. Maurya, and M. W. Khan, *NO, CO and H_2S based pharmaceuticals in the mission of vision (eye health): a comprehensive review*, Reviews in Inorganic Chemistry (to appear).

[47] R. R. Zaky, T. A. Yousef, and K. M. Ibrahim, *Co(II), Cd(II), Hg(II) and U(VI)O_2 complexes of o-hydroxyacetophenone[N-(3-hydroxy-2-naphthoyl)] hydrazone: Physicochemical study, thermal studies and antimicrobial activity*, Spectrochim Acta A Mol Biomol Spectrosc, 97 (2012), 683–694.

[48] D. Sun, W. Zhang, E. Yang, N. Li, H. Liu, and W. Wang, *Investigation of antibacterial activity and related mechanism of a ruthenium(II) polypyridyl complex*, Inorg Chem Commun, 56 (2015), 17–21.